

Hydrothermally Controlled Growth of $MnPO_4 \cdot H_2O$ Single-Crystal Rods

Yuanguang Zhang,[1,2] Yi Liu,[1,3] Shengquan Fu,[1] Fan Guo,[1] and Yitai Qian*[1]

[1]Structure Research Laboratory and Department of Chemistry, University of Science and Technology of China, Hefei 230026, P. R. China

[2]Department of Chemistry, Anqing Normal College, Anqing 246011, P. R. China

[3]Department of Chemistry, Zaozhuang University, Zaozhuang 277100, P. R. China

Received July 5, 2005; E-mail: ygz@mail.ustc.edu.cn

Rod-like $MnPO_4 \cdot H_2O$ single crystallites were hydrothermally prepared by the reaction of $Mn(NO_3)_2$ with H_3PO_4 at 130 °C for 16 h. The products were characterized by X-ray powder diffraction (XRD), transmission electron microscopy (TEM), infrared spectrum (IR), and their magnetic properties were evaluated on a vibrating sample magnetometer (VSM). The synthesized single-crystal rods have diameters of 0.1–0.66 μm and lengths of up to several micrometers. The influences of different phosphates, the volume ratio between reaction materials, reaction temperature, and reaction time on the morphology and phase of the final products under hydrothermal conditions are discussed. A possible formation mechanism has been proposed on the growth of $MnPO_4 \cdot H_2O$ single-crystal rods.

During the past decade, the preparation of open-framework metal phosphates has been extensively investigated, which might find applications in catalysis, adsorption, ionic conduction, or ion phosphates.[1–3] A large number of new metal phosphates with open-frameworks have been reported in the literature, such as gallium,[4] indium,[5,6] zinc,[7,8] iron,[9] tin,[10] vanadium,[11–13] molybdenum,[14] and cobalt phosphates.[15,16] Phosphates and arsenates of transition metals have been extensively studied due to their structural variability. Many of these materials are studied for their use as catalysts, ion exchangers, ionic conductors, or for intercalation reactions.[17] In the course of investigation of manganese phosphates, it was found that manganese phosphates and manganese phosphate hydrates are synthesized either by hydrothermal or by high temperature methods, and are also found in nature. Manganese has the most varied oxidation states of all of the elements. Materials of Mn^{3+}, Mn^{4+}, or both are widely used in batteries[18] and catalytic processes.[19–22] However, the reported manganese phosphates with open structures often contain Mn^{2+}.[23,24] One reason is the easy reduction of Mn^{3+} and/or Mn^{4+} materials to Mn^{2+} materials at high temperature. The other reason is the very low solubility of Mn^{3+} and Mn^{4+} in solution, which causes difficulties in the hydrothermal synthesis of open-structural materials with high-crystalline quality. Up to now, some studies on manganese(III) phosphates have been published. For instance, Mn(III)-compounds have been found and characterized by single crystal structure determination or from microcrystalline powders, such as MnP_3O_9,[25] $MnPO_4 \cdot H_2O$,[26] $MnPO_4 \cdot 0.962D_2O \cdot 0.038H_2O$,[27] $MnHP_2O_7$,[28] $Mn_3(PO_4)_2(OH)_2 \cdot 4H_2O$,[29] $KMn_2O(PO_4)(HPO_4)$,[30] $NH_4Mn_2O(PO_4)(HPO_4) \cdot H_2O$,[31] and $H_2MnP_3O_{10} \cdot 2H_2O$.[32] However, to the best of our knowledge, the growth of rod-like $MnPO_4 \cdot H_2O$ single crystallites has not been reported to date. The one-dimensional structures have attracted increasing attention as result of their novel physical and chemical properties.[33–35]

In this paper, we report a facile hydrothermal process to prepare rod-like $MnPO_4 \cdot H_2O$ single crystallites by the reaction of $Mn(NO_3)_2$ with H_3PO_4. A possible formation mechanism has been suggested.

Experimental

Preparation of Rod-Like $MnPO_4 \cdot H_2O$ Single Crystallites. All of the reagents used in the experiments were analytically pure and were purchased from Shanghai Chemical Reagent Company and were used without further purification. In a typical process, 5 mL of 50% $Mn(NO_3)_2$ and 30 mL of 98% H_3PO_4 were added to 10 mL of distilled water at room temperature to form a homogeneous solution, which was then transferred into a Teflon-lined stainless steel autoclave of 60 mL capacity. The autoclave was sealed and maintained at 130 °C for 16 h. Afterwards, the autoclave was allowed to cool to room temperature naturally. The pale-yellow products were collected by filtration, washed several times with distilled water and absolute ethanol to remove impurities, and then dried under vacuum at 60 °C for 3 h.

Characterization of Rod-Like $MnPO_4 \cdot H_2O$ Single Crystallites. X-ray powder diffraction (XRD) patterns were recorded on a Philips X'pert diffractometer using Cu Kα radiation (λ = 1.5418 Å). Transmission electron microscopy (TEM) images were taken using a Hitachi Model H-800 microscope. The infrared spectrum (IR) was recorded on a Bruker Vector-22 FT-IR sepectrometer from 400 to 4000 cm^{-1} at room temperature on KBr mulls. The magnetic properties were evaluated on a vibrating sample magnetometer (VSM). The samples used for characterization were dispersed in absolute ethanol and were ultrasonicated before TEM observation.

Results and Discussion

Structural and Morphologic Characterization of the Products. The XRD patterns of the products synthesized at different temperatures for 16 h are shown in Fig. 1. Figure 1a shows the XRD pattern of the product synthesized at 130 °C

Published on the web February 10, 2006; DOI 10.1246/bcsj.79.270

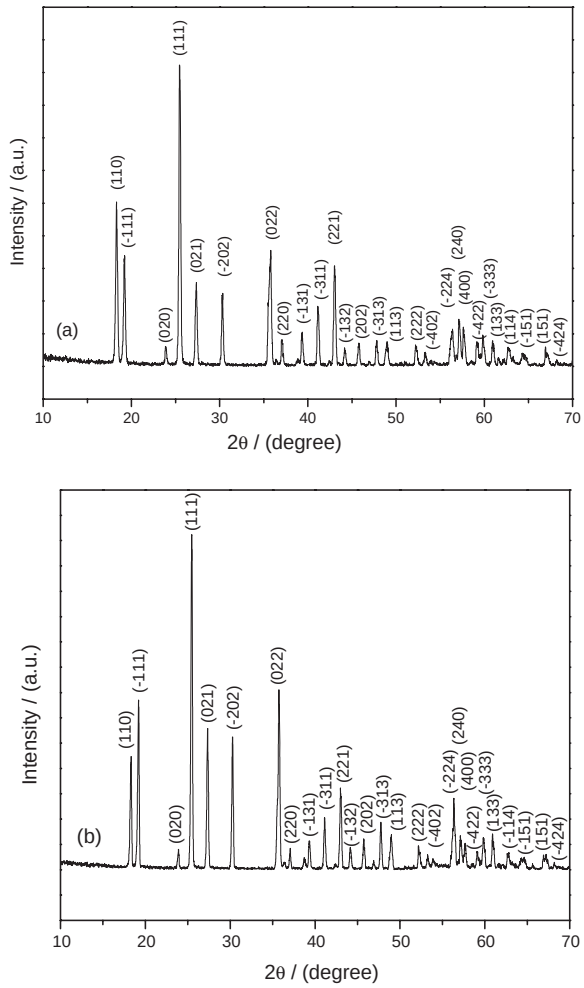

Fig. 1. XRD patterns of the as-prepared $MnPO_4 \cdot H_2O$ synthesized at different temperature for 16 h. (a) 130 °C; (b) 160 °C.

for 16 h. All of the reflections in this pattern can be readily indexed to a monoclinic phase [space group: $C2/c(15)$] of $MnPO_4 \cdot H_2O$ with the calculated lattice constants of $a = 6.910$ Å, $b = 7.473$ Å, $c = 7.355$ Å, which are in good agreement with the literature results (JCPDS No. 78-1082). No characteristic peaks of impurity phases are present, indicating the high purity of the final products. Figure 1b shows the XRD pattern of the product synthesized at 160 °C for 16 h. All of the reflections in this pattern can also be readily indexed to a monoclinic phase [space group: $C2/c(15)$] of $MnPO_4 \cdot H_2O$, which is consistent with the report (JCPDS No. 78-1082).

The IR spectrum of the product synthesized at 130 °C for 16 h is shown in Fig. 2. Three bands are observed in the region of hydroxy stretching. The main absorption band centered at 3096 cm^{-1} is typical of hydrogen phosphates and has been attributed to PO–H stretching.[36] The other bands situated at 3423 and 2922 cm^{-1} appear as shoulders: The first band is assigned to ν(HO–H) when the water interacts strongly through the hydrogen bonds. The second band can be assigned to either ν(MnO–H), $\nu(H_3O^+)$, or both.[37] The absorption band involving the triply degenerate asymmetric stretching vibrations of the isolated PO_4 tetrahedra is split into two bands, a doubly degenerated band at 1055 cm^{-1} and a nondegenerated band

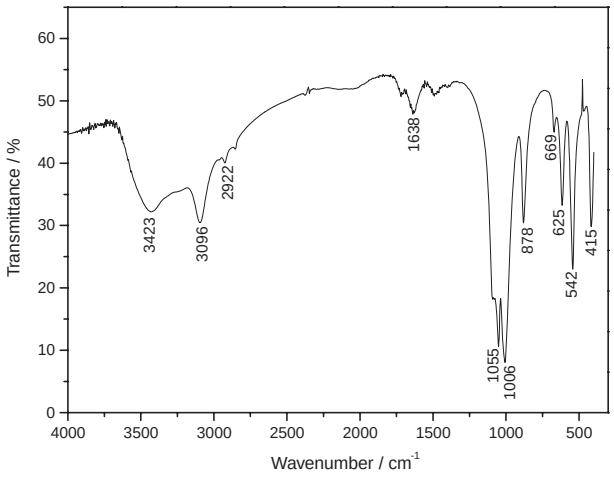

Fig. 2. IR spectrum of the as-prepared $MnPO_4 \cdot H_2O$ synthesized at 130 °C for 16 h.

at 1006 cm^{-1}. The bands centered at 878 and 669 cm^{-1} were assigned to the ν(P–OH) stretching and the δ(Mn–O–H) bending, respectively, due to the fact that they disappear in the heating process when the compound changes to anhydrous manganese(II) pyrophosphate; they are consistent with the different assignments for hydrogen phosphates given by Farmer.[38] The bands at 625, 542, and 415 cm^{-1} were assigned to δ(P–O–Mn), $\nu_4(PO_4)$, and ν(Mn–OP), respectively, according to the literatures.[36,38] A conspicuous band can be observed at 1638 cm^{-1}, which is attributed to the deformation vibration of the species H_3O^+.[37]

The morphologies and microstructures of the as-prepared $MnPO_4 \cdot H_2O$ were investigated using the TEM technique. Figures 3a and 3b show TEM images of the as-prepared $MnPO_4 \cdot H_2O$ synthesized at 130 °C for 16 h. From these images, it was found that the products of $MnPO_4 \cdot H_2O$ were mostly composed of rod-like structures. These rods have diameters of 0.1–0.66 μm and lengths of up to several micrometers. The corresponding SAED (selected-area electron diffraction) pattern of a single $MnPO_4 \cdot H_2O$ rod is shown in the inset of Fig. 3a. This pattern displays many diffraction spots, indicating that these $MnPO_4 \cdot H_2O$ products exhibit single-crystal nature. Figure 3c shows a TEM image of the as-prepared $MnPO_4 \cdot H_2O$ synthesized at 160 °C for 16 h. From this image, it was found that most of the products display irregular rods with larger diameters.

Experimental Conditions of the $MnPO_4 \cdot H_2O$ Products. In the present experiment, the possible chemical reactions can be formulated as follows:

$$Mn(NO_3)_2 + H_3PO_4 \rightarrow MnPO_4 \cdot H_2O + NO_2 + HNO_3. \quad (1)$$

According to Eq. 1, $Mn(NO_3)_2$ is both the oxidant and reductant in the redox reaction. Under acidic conditions, the oxidation capability of the NO_3^- ion could be increased. On the other hand, due to the formation of both $MnPO_4 \cdot H_2O$ precipitation and NO_2 gas, Mn^{2+} could be oxidized to Mn^{3+} by the NO_3^- ion, then formed $MnPO_4 \cdot H_2O$ with H_3PO_4. The reaction (1) can proceed toward the right-hand side. Equation 1 suggests that the reaction (1) is affected by the concentration of H_3PO_4, which not only affects the oxidation capability of the NO_3^- ion, but also affects the formation rate of $MnPO_4 \cdot$

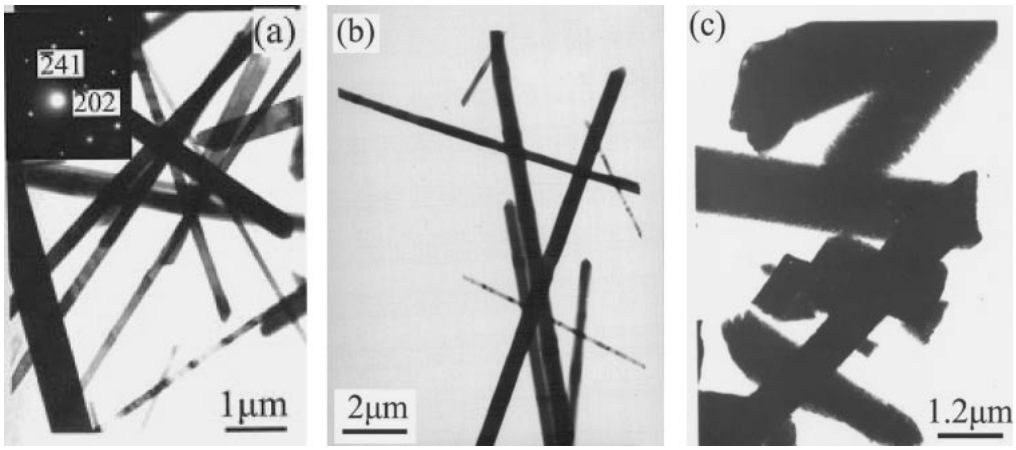

Fig. 3. TEM images of the as-prepared $MnPO_4 \cdot H_2O$ synthesized at different temperature for 16 h. (a) and (b) 130 °C; (c) 160 °C.

Table 1. Experimental Conditions of the Products

Sample no.	$Mn(NO_3)_2$ /mL	H_3PO_4 /mL	H_2O /mL	Reaction temperature/°C	Reaction time/h	Product composition
1	5	15	25	130	16	$MnPO_4 \cdot H_2O$
2	5	20	20	130	16	$MnPO_4 \cdot H_2O$
3	5	30	10	130	16	$MnPO_4 \cdot H_2O$
4	5	35	5	130	16	$MnPO_4 \cdot H_2O$
5	5	30	10	130	12	$MnPO_4 \cdot H_2O$
6	5	30	10	130	8	$MnPO_4 \cdot H_2O$
7	5	30	10	130	4	$MnPO_4 \cdot H_2O$
8	5	30	10	90	16	no $MnPO_4 \cdot H_2O$
9	5	30	10	110	16	no $MnPO_4 \cdot H_2O$
10	5	30	10	160	16	$MnPO_4 \cdot H_2O$

H_2O. Thus, it is important to select appropriate concentration of H_3PO_4 in the experiment.

In the present experiment, the system only contained three components: $Mn(NO_3)_2$, H_3PO_4, and H_2O. Keeping the total volume of the reaction media unchanged, we made some experiments by changing reaction temperature, reaction time, and the concentration of H_3PO_4. Detailed experimental conditions are listed in Table 1.

Influences of the Amount of H_3PO_4 and Temperature: From keeping the reaction temperature (130 °C) and time (16 h) unchanged, a series of experiments were made by changing the volume ratio of $Mn(NO_3)_2$ to H_3PO_4 (1:3, 1:4, 1:6, and 1:7), respectively, as seen in Table 1. It was found that the volume ratio of $Mn(NO_3)_2$ to H_3PO_4 has almost no influence on the formation of the $MnPO_4 \cdot H_2O$ phase; it only affects the morphology of $MnPO_4 \cdot H_2O$. When the volume ratio of $Mn(NO_3)_2$ to H_3PO_4 is 1:3, 1:4, 1:6, or 1:7, it was found that all of the products could be indexed to pure $MnPO_4 \cdot H_2O$ phases, which could be demonstrated from the XRD results (Fig. 4 and Fig. 1a). Compared to the diffraction intensity of (110) and (−111) as shown in Fig. 4 and Fig. 1a, respectively, it was found that with the increase of the volume ratio of $Mn(NO_3)_2$ to H_3PO_4 (1:3, 1:4, 1:6, and 1:7), the diffraction intensity of (110) gradually strengthened, while that of (−111) gradually weakened, which suggested that the growth orientation of $MnPO_4 \cdot H_2O$ rods is affected by the volume ratio of $Mn(NO_3)_2$ to H_3PO_4. The morphologies of the products synthesized at volume ratios of 1:3, 1:4, and 1:7 are shown in Fig. 5. From the TEM images, it was found that these products show rod-like morphologies, but with some defects in these rods. Our experiments confirmed that the volume ratio of $Mn(NO_3)_2$ to H_3PO_4 of 1:6 was suitable for the formation of rod-like $MnPO_4 \cdot H_2O$ single crystallites (Figs. 3a and 3b). In addition, it was found that reaction temperature has a significant influence on the formation of rod-like $MnPO_4 \cdot H_2O$ single crystallites. When the reaction temperature was either 90 or 110 °C, no $MnPO_4 \cdot H_2O$ products were obtained, while when

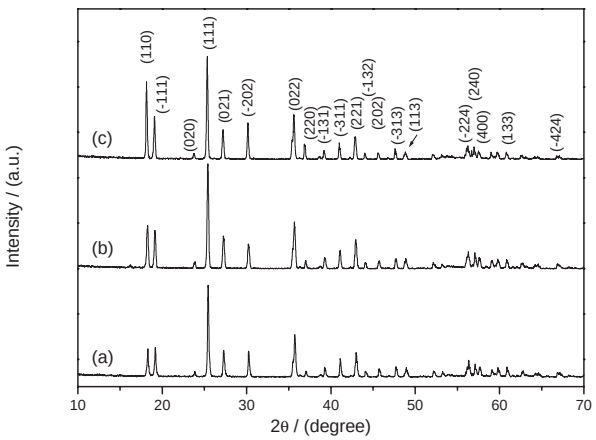

Fig. 4. XRD patterns of the as-prepared $MnPO_4 \cdot H_2O$ synthesized at 130 °C for 16 h at different volume ratio. (a) 1:3; (b) 1:4; (c) 1:7.

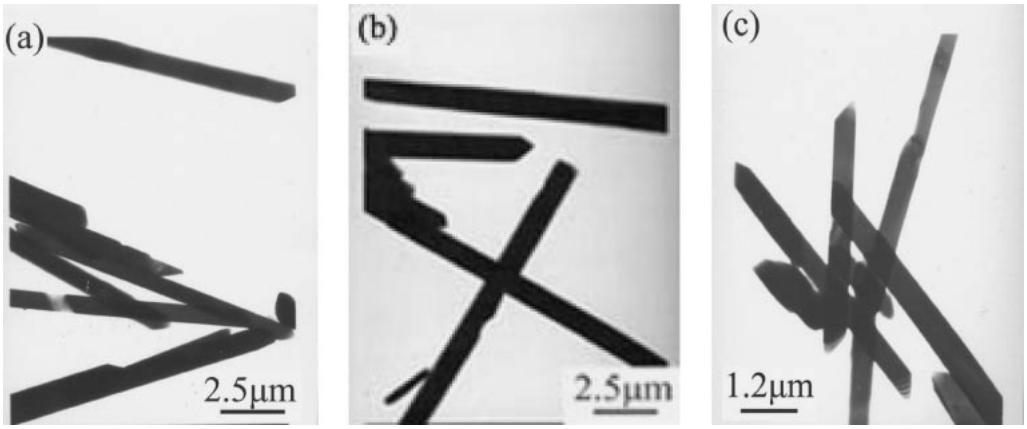

Fig. 5. TEM images of the as-prepared $MnPO_4 \cdot H_2O$ synthesized at 130 °C for 16 h at different volume ratio. (a) 1:3; (b) 1:4; (c) 1:7.

the reaction temperature was raised to 130 or 160 °C, the pure phase of $MnPO_4 \cdot H_2O$ was afforded.

Influences of Reaction Time: As seen in Table 1, we selected the volume ratio of $Mn(NO_3)_2$ to H_3PO_4 of 1:6, and kept all other reaction conditions unchanged by only changing the reaction time for 4, 8, 12, and 16 h, respectively. The XRD results (Fig. 6) show that all products synthesized at 4, 8, or 12 h could be indexed to pure $MnPO_4 \cdot H_2O$ phases. The TEM images (Fig. 7) indicate that these products display mostly rod-like morphologies. As the reaction time increased from 4 to 16 h, the average diameters of $MnPO_4 \cdot H_2O$ rods decreased, while the morphologies of $MnPO_4 \cdot H_2O$ rods changed from irregular to regular. It shows that the morphologies of these products are significantly influenced by reaction time. The SAED pattern (inset of Fig. 7a) of the product synthesized at 4 h displays a single-crystalline spot, which can be indexed to the $MnPO_4 \cdot H_2O$ phase.

Influences of Phosphate: In the present study, we found that H_3PO_4 is irreplaceable for the formation of rod-like $MnPO_4 \cdot H_2O$ single crystallites at 130 °C for 16 h. When other phosphates, such as $NH_4H_2PO_4$, NaH_2PO_4, or H_3PO_3, were used instead of H_3PO_4, no $MnPO_4 \cdot H_2O$ was obtained. When Na_3PO_4 or $Na_2P_2O_7$ was used instead of H_3PO_4, no pure $MnPO_4 \cdot H_2O$ phases were obtained, which can be demonstrated from the XRD results.

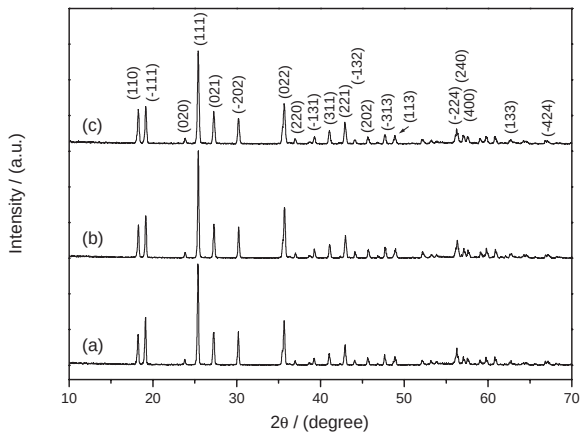

Fig. 6. XRD patterns of the as-prepared $MnPO_4 \cdot H_2O$ synthesized at 130 °C for different time. (a) 4 h; (b) 8 h; (c) 12 h.

Possible Formation Mechanism of the $MnPO_4 \cdot H_2O$ Single-Crystal Rods. Based on the above experimental results and $MnPO_4 \cdot H_2O$ crystal structure, we suggest a possible formation mechanism of the as-prepared $MnPO_4 \cdot H_2O$ single-crystal rods. The $MnPO_4 \cdot H_2O$ structure consists of a network of MnO_6 octahedra and PO_4 tetrahedra linked together by

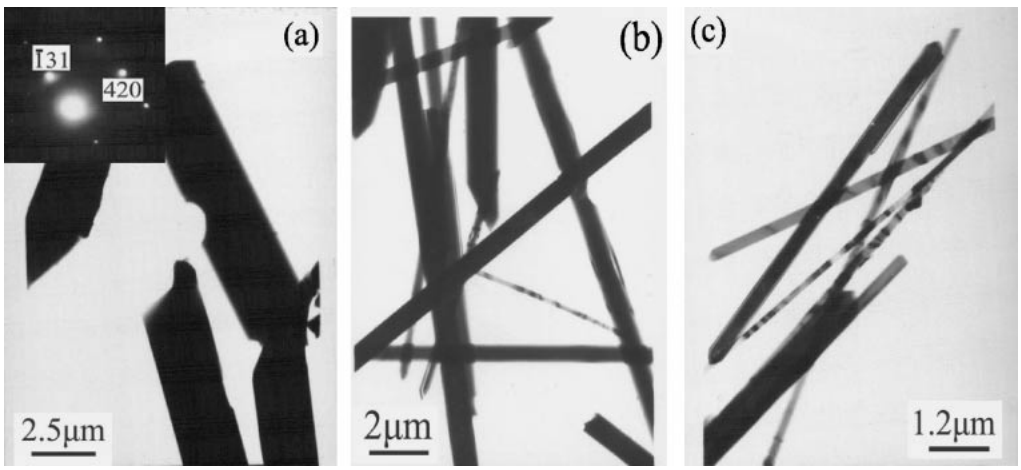

Fig. 7. TEM images of the as-prepared $MnPO_4 \cdot H_2O$ synthesized at 130 °C for different time. (a) 4 h; (b) 8 h; (c) 12 h.

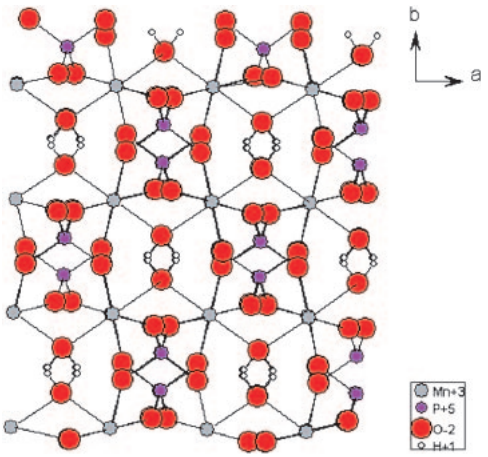

Fig. 8. Project of the structure along *c* direction.

vertex sharing into a continuous three-dimensional array. *trans*–Mn–O–Mn-chains run parallel to the 101 direction, the oxygen atom of the water molecule being at the vertex of two adjacent MnO_6 octahedra. These chains are interconnected by PO_4 groups such that the resulting framework encloses small channels running parallel to the *c* axis, into which the H atoms of the water molecules project (Fig. 8). The PO_4 tetrahedron is almost regular, whereas the MnO_6 octahedron shows a considerable tetragonal distortion. The high-spin Mn(III) ion has a $t_{2g}^3e_g^1$ electronic configuration and hence is expected to show a Jahn–Teller distortion.[26] This structure is perhaps favorable to the growth of $MnPO_4 \cdot H_2O$ single-crystal rods. There have been some reports describing the relation between the material crystal-structure change and the Jahn–Teller effect. For example, a single-crystal $Ca_3Mn_2Ge_3O_{12}$ garnet structure has two different Jahn–Teller distorted MnO_6 octahedra, with a different orientation of the axis of polyhedral elongation. The ordering scheme of these Jahn–Teller distorted octahedra follows in an alternating pattern the densest rod packing, and the cooperative effect of the electronically induced octahedral distortion was found to be responsible for the cubic-to-tetragonal symmetry breaking in the $Ca_3Mn_2Ge_3O_{12}$ garnet, and thus is responsible for the overall lower symmetry.[39] Experimental and theoretical investigation on the relative stability of the PdS_2- and pyrite-type structures of $PdSe_2$ showed that the structural change of $PdSe_2$ from the pyrite-type to the PdS_2-type structure can be regarded as a "Jahn–Teller" distortion of each $PdSe_6$ octahedron.[40] Variable-temperature single-crystal neutron diffraction structures of the alums $CsM^{III}(SO_4)_2 \cdot 12D_2O$, where M(III) is Ti, V, Mn, or Ga, are reported. The titanium and manganese alums undergo cubic to orthorhombic phase transitions at certain temperatures. This structural instability exhibited by these salts is interpreted as arising from cooperative Jahn–Teller interactions.[41] In addition, the essential role of strain in determining the electronic states of perovskite manganites is clearly demonstrated in the form of anisotropic and substrate-dependent crossover of a first-order phase transition in charge orbital ordered epitaxial thin films of $(Nd_{1-x}Pr_x)_{0.5}Sr_{0.5}MnO_3$. The substrate-induced strain is a powerful tool for the control of the metal-insulator transition by tuning the one-electron bandwidth through the Jahn–Teller distortion.[42] Although there is no report describing that the formation of single crystalline $MnPO_4 \cdot H_2O$ rods has some relation to the Jahn–Teller effect, it can be deduced that the formation of single crystalline $MnPO_4 \cdot H_2O$ rods is affected by the $MnPO_4 \cdot H_2O$ crystal structure. In our experiments, there are no other factors, such as hard templates or soft templates, that can affect the shape of the $MnPO_4 \cdot H_2O$ crystal.

In the initial stage of the reaction, the nucleation rate of $MnPO_4 \cdot H_2O$ in the autoclave might be slow because of the low concentration of Mn^{3+}. Therefore, rod-like $MnPO_4 \cdot H_2O$ single crystallites with larger diameters could be formed. It was suggested that a condensation reaction plays a key role in the formation of nanowires of Mn-based compounds.[43] Under hydrothermal conditions, the MnO_x units form first in solution, and then form kelp-shaped films via a condensation reaction. During the condensation process, kelp-shaped films grow into nanowires. This model is also applicable to the formation of $MnPO_4 \cdot H_2O$ nanorods in our system. The main difference is that the solution becomes more acidic owing to the formation of HNO_3 in the system, which leads to the decrease of the concentration of MnO_x units and the recrystallization of $MnPO_4 \cdot H_2O$ nanorods. As a result, $MnPO_4 \cdot H_2O$ rods with smaller diameters would be formed after longer hydrothermal treatment. Although the phases of initial and resulting $MnPO_4 \cdot H_2O$ products are the same, the growth orientation of $MnPO_4 \cdot H_2O$ single crystallite rods might be different. One reason is that the peak-intensity ratio of (110) to (−111) becomes larger as the reaction time increases from 4 to 16 h (Fig. 6 and Fig. 1a), which might suggest the change of growth orientation of $MnPO_4 \cdot H_2O$ rods. Another reason is that the crystal belt axis of the initial and resulting $MnPO_4 \cdot H_2O$ single-crystal rods is [414] and [127] from the insets of Fig. 3a and Fig. 7a, respectively. Further discussion about the growth orientation of the initial or resulting $MnPO_4 \cdot H_2O$ single-crystal rods would be difficult by the electron-diffraction method, because the $MnPO_4 \cdot H_2O$ single-crystal rods are sensitive to electron beams. Although other unknown factors may exist that influence the growth of rod-like $MnPO_4 \cdot H_2O$ single crystallites, such as the influence of anions, the above mechanism is in good agreement with our experiment results.

Magnetic Properties of the $MnPO_4 \cdot H_2O$ Products. Figure 9 shows room temperature M–H hysteretic loops of the products synthesized at different temperatures for 16 h with an external magnetic field applied. Form the pattern, we know that the coercivity values Hc for the samples synthesized at 130 and 160 °C are 465 and 544 Oe, respectively. Up to now, there have been no reports describing $MnPO_4 \cdot H_2O$ as a ferromagnet at room temperature. The two-dimensional manganese alkylphosphonate hydrates $MnC_nH_{2n+1}PO_3 \cdot H_2O$ show only weak ferromagnetization at low temperatures.[44] The possible existence of impurities such as Mn_3O_4 might be responsible for the room temperature magnetic properties of the samples.

Conclusion

Single-crystal $MnPO_4 \cdot H_2O$ rods with diameters of 0.1–0.66 μm and lengths of up to several micrometers have been hydrothermally synthesized at low temperatures. It was found that selection of the appropriate reaction temperature, reaction time, and kind of phosphate is crucial for the formation of $MnPO_4 \cdot H_2O$ single-crystal rods. The suggested growth mech-

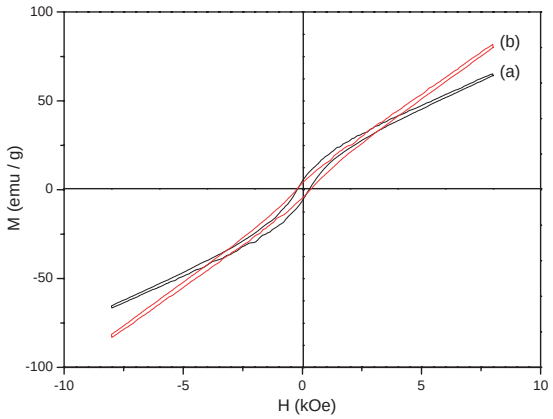

Fig. 9. The room temperature M–H hysteretic loops of the as-prepared $MnPO_4 \cdot H_2O$ synthesized at different temperature for 16 h with an external magnetic field applied. (a) 130 °C; (b) 160 °C.

anism of single-crystal $MnPO_4 \cdot H_2O$ rods is in good agreement with our experimental results. This low-temperature synthetic route might be a general one for the growth of other single-crystal metal phosphates with one-dimensional structures.

This work was supported by the National Natural Science Foundation of China and the 973 Project of China.

References

1 S. T. Wilson, B. M. Lok, C. A. Messina, T. R. Cannan, E. M. Flanigen, *J. Am. Chem. Soc.* **1982**, *104*, 1146.
2 M. E. Davis, C. Saldarriage, C. Montes, J. Garces, C. Crowder, *Nature* **1988**, *331*, 698.
3 J. Chen, W. Pang, R. Xu, *Top. Catal.* **1999**, *9*, 93.
4 R. Xu, J. Chen, S. Feng, *Stud. Surf. Sci. Catal.* **1991**, *60*, 63.
5 I. D. Williams, J. Yu, H. Du, J. Chen, W. Pang, *Chem. Mater.* **1998**, *10*, 773.
6 S. S. Dhingra, R. C. Haushalter, *J. Chem. Soc., Chem. Commun.* **1993**, 1665.
7 W. T. A. Harrison, T. E. Martin, T. E. Gier, G. D. Stucky, *J. Mater. Chem.* **1992**, *2*, 175.
8 G. Yang, S. C. Sevov, *J. Am. Chem. Soc.* **1999**, *121*, 8389.
9 K. Lii, Y. Huang, V. Zima, C. Huang, H. Lin, Y. Jiang, F. Liao, S. Wang, *Chem. Mater.* **1988**, *10*, 2599.
10 S. Natarajan, S. Ayyappan, A. K. Cheetham, C. N. R. Rao, *Chem. Mater.* **1998**, *10*, 1627.
11 Y. Zhang, A. Clearfield, R. C. Haushalter, *Chem. Mater.* **1995**, *7*, 1221.
12 Z. Bircask, W. T. A. Harrison, *Inorg. Chem.* **1998**, *37*, 3204.
13 M. I. Khan, L. M. Meyer, R. C. Haushalter, A. L. Schweizter, J. Zubieta, J. L. Dye, *Chem. Mater.* **1996**, *8*, 43.
14 R. C. Haushalter, L. A. Mundi, *Chem. Mater.* **1992**, *4*, 31.
15 J.-S. Chen, R. H. Jones, S. Natarajan, M. B. Hursthouse, J. M. Thomas, *Angew. Chem., Int. Ed. Engl.* **1994**, *33*, 639.
16 P. Feng, X. Bu, G. D. Stucky, *Nature* **1997**, *388*, 735.
17 A. K. Cheetham, G. Férey, T. Loiseau, *Angew. Chem.* **1999**, *111*, 3466; *Angew. Chem., Int. Ed.* **1999**, *38*, 3268.
18 Y. Chabre, J. Pannetier, *Prog. Solid State Chem.* **1995**, *23*, 1.
19 V. V. Krishnan, S. L. Suib, *J. Catal.* **1999**, *184*, 305.
20 H. Zhou, Y. F. Shen, J. Y. Wang, X. Chen, C.-L. O'Young, S. L. Suib, *J. Catal.* **1998**, *176*, 321.
21 G. G. Xia, Y. G. Yin, W. S. Willis, J. Y. Wang, S. L. Suib, *J. Catal.* **1999**, *185*, 91.
22 J. Luo, Q. Zhang, A. Huang, S. L. Suib, *Microporous Mesoporous Mater.* **2000**, *35*, 209.
23 A. Daidouh, J. L. Martinez, C. Pico, M. L. Veiga, *J. Solid State Chem.* **1999**, *144*, 169.
24 J. Escobal, J. L. Mesa, J. L. Pizarro, L. Lezama, R. Olazcuaga, T. Rojo, *J. Mater. Chem.* **1999**, *9*, 2691.
25 M. Bagieu-Beucher, *Acta Crystallogr., Sect. B* **1978**, *34*, 1443.
26 P. Lightfoot, A. K. Cheetham, A. W. Sleight, *Inorg. Chem.* **1987**, *26*, 3544.
27 M. A. G. Aranda, J. P. Attfield, S. Bruque, F. Palacio, *J. Mater. Chem.* **1992**, *2*, 501.
28 A. Durif, M. T. Averbuch-Pouchot, *Acta Crystallogr., Sect. B* **1982**, *38*, 2883.
29 A. R. Kampk, P. B. Moore, *Am. Mineral.* **1976**, *61*, 1241.
30 P. Lightfoot, A. K. Cheetham, A. W. Sleight, *J. Solid State Chem.* **1988**, *73*, 325.
31 P. Lightfoot, A. K. Cheetham, *J. Solid State Chem.* **1988**, *78*, 17.
32 M. A. G. Aranda, S. Bruque, J. P. Attfield, *Inorg. Chem.* **1991**, *30*, 2043.
33 *Handbook of Nanostructured Materials and Nanotechnology*, ed. by H. S. Nalwa, Academic Press, New York, **2000**.
34 J. Hu, T. W. Odom, C. M. Lieber, *Acc. Chem. Res.* **1999**, *32*, 435.
35 Z. L. Wang, *Adv. Mater.* **2000**, *12*, 1295.
36 K. Nakamoto, in *Infrared Spectra of Inorganic and Coordination Compounds*, 2nd ed., Wiley-Interscience, New York, **1970**.
37 P. Remy, J. Fraissard, A. Biolle, *Bull. Soc. Chim. Fr.* **1968**, 2222.
38 V. C. Farmer, in *The Infrared Spectra of Minerals*, Mineralogical Society London, **1974**.
39 S. Heinemann, R. Miletich, *Am. Mineral.* **2000**, *85*, 993.
40 C. Soulard, X. Rocquefelte, P. E. Petit, M. Evain, S. Jobic, J. P. Itie, P. Munsch, H. J. Koo, M. H. Whangbo, *Inorg. Chem.* **2004**, *43*, 1943.
41 P. L. W. Tregenna-Piggott, H.-P. Andres, G. J. McIntyre, S. P. Best, C. C. Wilson, J. A. Cowan, *Inorg. Chem.* **2003**, *42*, 1350.
42 Y. Ogimoto, M. Nakamura, N. Takubo, H. Tamaru, M. Izumi, K. Miyano, *Phys. Rev. B* **2005**, *71*, 060403(R).
43 W. Mingdeng, K. Yoshinari, Z. Haoshen, S. Hideki, A. Hironori, *Nanotechnology* **2005**, *16*, 245.
44 S. G. Carling, P. Day, D. Visser, *J. Phys.: Condens. Matter* **1995**, *7*, 109.